Scanning tunneling spectrum of electrons confined in a rectangular quantum corral

2009 J. Phys.: Condens. Matter 21 225004

(http://iopscience.iop.org/0953-8984/21/22/225004)

J. Phys.: Condens. Matter **21** (2009) 225004 (7pp) doi:10.1088/0953-8984/21/22/225004

Scanning tunneling spectrum of electrons confined in a rectangular quantum corral

Takuya Kumagai and Akira Tamura[1]

Faculty of Materials Science, Graduate School, Saitama Institute of Technology, 1690 Fusaiji, Fukaya City, 369-0293 Saitama, Japan

Received 3 January 2009, in final form 26 March 2009
Published 22 April 2009
Online at stacks.iop.org/JPhysCM/21/225004

Abstract

We obtained the scanning tunneling spectrum (STS) of an electron confined in a rectangular quantum corral by considering the electron to be in a quasi-stationary state. Because of non-hermiticity of the Hamiltonian, the electron has a complex eigenenergy. The imaginary part gives the peak width coming mainly from the electron tunneling through a corral barrier. Our STS is consistent with the experimental spectrum that had been measured for electrons confined in a rectangular quantum corral. We obtained peak widths against energy levels and components of the STS which are constructed with quasi-stationary eigenstates. It is shown that normalization of a wavefunction by considering its time evolution is decisive in obtaining the proper STS. Moreover, we specified the position dependence of STS in relation to the image of the surface local density of states.

1. Introduction

On noble metal surfaces such as Cu, Ag and Au, there exists a Shockley electron that has a parabolic band located in the bulk bandgap [1]. The Shockley electron freely moves in a parallel direction to the surface but it is localized in the normal direction to the surface. By making use of scanning tunneling microscopy (STM), Eigler's group [2–7] developed a new field of study that enables us to fabricate an artificial system in a nanoscale. They clearly showed the wave feature of Shockley electrons confined in a circular quantum corral (QC) built up with 48 iron atoms on a Cu(111) surface. Since then many researchers have been promoting studies on several kinds of QCs or quantum islands fabricated on noble metal and transition metal surfaces [8–12]. In those experiments STM images have been observed in topographical or differential conductance modes. Moreover, a scanning tunneling spectrum (STS) has been measured [4–6, 8–10] to clarify the characteristic energy levels and energy widths of electrons confined in QCs. The inverse of energy width gives the lifetime of an electron staying within a QC. Hence, by use of an STM apparatus, we can obtain information on confined electrons in both real space and energy space.

As regards theoretical analyses there are several approaches. One is based on a scattering theory in which electron waves scattered from corral atoms construct a density profile inside a QC [5, 6, 9, 12, 13]. Each scattered wave has a circular symmetry around the corral atom. By superimposing such scattered waves they derived the local density of states (LDOS) from a Green's function. Another is based on a viewpoint that confined electrons are in stationary states in a QC [8, 10, 14, 15]. In reality, such electrons leak out of the well by tunneling through the corral barrier, which makes the lifetime of the electron and peak widths of STS finite. However, we cannot pick out each peak width when experimental peaks are not separated. Several researchers introduced energy widths from experimental peak profiles of STS. Kliewer *et al* [9] used experimental energy widths measured for a circular QC formed on an Ag(111) surface. From another viewpoint that a confined electron is in a quasi-stationary state, we naturally derive the lifetime of the electron and the LDOS which can be measured by STS, and analyze the experimental STS.

2. Quasi-stationary states

2.1. One-dimensional quasi-stationary state

At first we consider a quasi-stationary state for a one-dimensional QC. Figure 1 shows a schematic image of the potential energy where E_F means the Fermi level.

The Schrödinger equation for the present system can be written as

$$i\hbar\frac{\partial}{\partial t}\Psi(x,t) = \left[-\frac{\hbar^2}{2m^*}\frac{\partial^2}{\partial x^2} + V(x)\right]\Psi(x,t) = E\,\Psi(x,t). \quad (1)$$

[1] Author to whom any correspondence should be addressed.

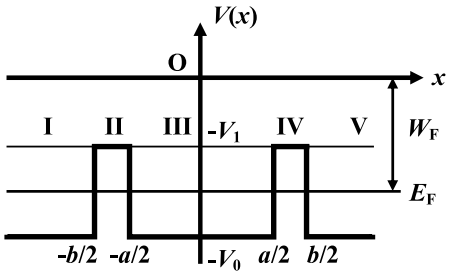

Figure 1. One-dimensional potential energy whose barrier width is finite.

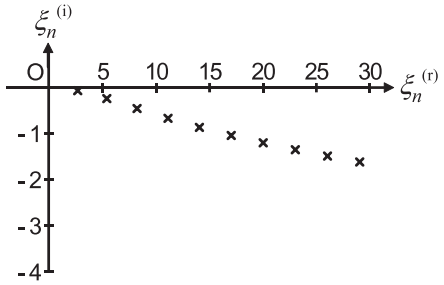

Figure 2. Distribution of complex wavenumbers $\xi_n = k_n a$: $n = 1$–10.

By pulling out a time-dependent term from a wavefunction, $\Psi(x,t) = \psi(x)\exp(-\mathrm{i}Et/\hbar)$, $\psi(x)$ satisfies the following Schrödinger equation:

$$H\psi(x) = \left[-\frac{\hbar^2}{2m^*}\frac{\partial^2}{\partial x^2} + V(x)\right]\psi(x) = E\psi(x). \quad (2)$$

Here we consider the case in which an electron is initially supplied in region III. Such an electron occupies an energy level higher than E_F and fades away from the QC. Hence, we assign wavefunctions in regions from I to V as follows; $\psi_\mathrm{I}(x) = A\exp(-\mathrm{i}kx)$, $\psi_\mathrm{II}(x) = B\exp(qx) + C\exp(-qx)$, $\psi_\mathrm{III}(x) = D\sin kx + F\cos kx$, $\psi_\mathrm{IV}(x) = G\exp(qx) + H\exp(-qx)$ and $\psi_\mathrm{V}(x) = J\exp(\mathrm{i}kx)$. In regions I and V, we consider electron waves outgoing from the QC because there is no wave incoming into the QC. A whole wavefunction can be classified into a symmetric or an antisymmetric wavefunction because our potential energy is symmetric with respect to a $V(x)$ axis.

To derive eigenvalues of k, we impose boundary conditions that the wavefunction and its first derivative are continuous at four boundaries; $x = \pm a/2$ and $\pm b/2$. We obtained the following two kinds of eigenvalue equation:

$$q\cos\frac{1}{2}ka - k\sin\frac{1}{2}ka = \mathrm{e}^{-q(b-a)}\frac{q+\mathrm{i}k}{q-\mathrm{i}k} \times (q\cos\tfrac{1}{2}ka + k\sin\tfrac{1}{2}ka). \quad (3)$$

for the symmetric wavefunction and

$$k\cos\frac{1}{2}ka + q\sin\frac{1}{2}ka = -\mathrm{e}^{-q(b-a)}\frac{q+\mathrm{i}k}{q-\mathrm{i}k} \times (k\cos\tfrac{1}{2}ka - q\sin\tfrac{1}{2}ka), \quad (4)$$

for the antisymmetric wavefunction. Equations (3) and (4) are invariant under simultaneous transformations $k \to -k$ and $q \to -q$. In the limit $b \to \infty$, we reproduce eigenvalue equations for stationary states whose k and q are real numbers. Because of an imaginary unit 'i' included in equations (3) and (4), eigenvalues become complex numbers. By making both k and q be $k = k^{(\mathrm{r})} + \mathrm{i}k^{(\mathrm{i})}$ and $q = q^{(\mathrm{r})} + \mathrm{i}q^{(\mathrm{i})}$, we numerically solved equations (3) and (4) with another relation $k^2 + q^2 = (2m^*/\hbar^2)(V_0 - V_1)$. The eigenenergy defined by $E_n = [\hbar^2/(2m^*)]k_n^2 - V_0$ can be written as a complex number $E_n = E_n^{(\mathrm{r})} - \frac{1}{2}\mathrm{i}\Gamma_n$, where $E_n^{(\mathrm{r})} = [\hbar^2/(2m^*)][{k_n^{(r)}}^2 - {k_n^{(i)}}^2] - V_0$ and $\Gamma_n = (2\hbar^2/m^*)k_n^{(\mathrm{r})}|k_n^{(\mathrm{i})}|$.

Figure 2 shows the distribution of complex wavenumbers expressed as non-dimensional values $\xi_n = k_n a = \xi_n^{(\mathrm{r})} + \mathrm{i}\xi_n^{(\mathrm{i})}$, where we chose $a = 90$ Å $- d$, $b = 90$ Å $+ d$ and $d = \frac{1}{2}(b-a) = 2.74$ Å; a diameter of an Mn atom [16, 17]. Crosses represent poles of wavenumbers on a complex plane. The imaginary part $k_n^{(\mathrm{i})}$ is negative.

Considering these situations, we propose a new normalization method of $\Psi(x,t)$ taking account of the time dependence of a quasi-stationary state. Here we define $\Phi_n(x,t)$ which satisfies a relation $\Psi_n(x,t) = \exp(-\mathrm{i}E_\mathrm{F}t/\hbar)\Phi_n(x,t)$. When the bias voltage of the STM tip is positive with respect to E_F, an electron supplied in the QC occupies a quasi-stationary energy level higher than E_F. $\Phi_n(x,t)$ represents the state having the energy $E - E_\mathrm{F}$. The $\Phi_n(x,t)$ moving from the well to the far right can be written as

$$\Phi_{\mathrm{V}n}(x,t) = A\exp\{\mathrm{i}[k_n^{(\mathrm{r})}x - (E_n^{(\mathrm{r})} - E_\mathrm{F})t/\hbar]\} \times \exp[|k_n^{(\mathrm{i})}|(x - \upsilon_n^{(\mathrm{r})}t)]. \quad (5)$$

A term $\exp[|k_n^{(\mathrm{i})}|(x - \upsilon_n^{(\mathrm{r})}t)]$ plays the role of an envelope specified by $k_n^{(\mathrm{i})}$ and Γ_n. In the limit $x \to +\infty$, $\Phi_{\mathrm{V}n}(x,t)$ diverges. Because $\Phi_{\mathrm{V}n}(x,t)$ has a wavefront at $x = \upsilon_n^{(\mathrm{r})}t$, we normalize $|\Phi_{\mathrm{V}n}(x,t)|^2$ and $|\Psi_{\mathrm{V}n}(x,t)|^2$ in the region from $\frac{1}{2}b$ to $\upsilon_n^{(\mathrm{r})}t$. This comes from a situation that the outgoing wave cannot pull ahead of the wavefront. At a finite time t, we define the probability in each region as

$$W_{Nn}(t) = \int_N |\Psi_n(x,t)|^2\,\mathrm{d}x. \quad (6)$$

A label N represents a region over which we carry out integration. The probability of an electron which exists in region V can be obtained as

$$W_{\mathrm{V}n}(t) = \int_{b/2}^{\upsilon^{(\mathrm{r})}t} |J_n|^2\exp[2|k_n^{(\mathrm{i})}|(x - \upsilon_n^{(\mathrm{r})}t)]\,\mathrm{d}x = \frac{|J_n|^2}{2|k_n^{(\mathrm{i})}|}\left\{1 - \exp\left[-2|k_n^{(\mathrm{i})}|\left(\upsilon_n^{(\mathrm{r})}t - \frac{1}{2}b\right)\right]\right\}. \quad (7)$$

Actually it takes a long time to gain data for the STM current so that a condition $t \gg b/(2\upsilon_n^{(\mathrm{r})})$ is fulfilled. Hence, we can apply a limiting case $t \to \infty$ to the present system, which makes $W_{\mathrm{II}n}(t)$, $W_{\mathrm{III}n}(t)$ and $W_{\mathrm{IV}n}(t)$ be negligible and makes $W_{\mathrm{I}n}(t)$ and $W_{\mathrm{V}n}(t)$ be independent of time. We normalize the whole wavefunction, therefore, so that both $W_{\mathrm{I}n}(+\infty)$ and $W_{\mathrm{V}n}(+\infty)$ are $\frac{1}{2}$, which yields $|A_n| = \sqrt{|k_n^{(\mathrm{i})}|}$ and $|J_n| = \sqrt{|k_n^{(\mathrm{i})}|}$ because an electron runs away toward the far left or

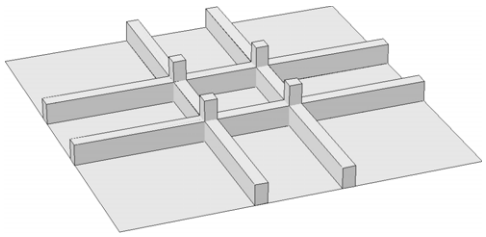

Figure 3. Schematic 3D illustration of our rectangular QC.

the far right with the same probability $\frac{1}{2}$. If $t \approx b/(2v_n^{(\mathrm{r})})$ shortly after wavefronts appear from barrier walls, coefficients A_n and J_n depend on time. It is inadequate to apply our normalization procedure to this span of time because the wavefunction $\Psi(x,t)$ does not satisfy equation (1). Our choice that $|A_n| = \sqrt{|k_n^{(\mathrm{i})}|}$ and $|J_n| = \sqrt{|k_n^{(\mathrm{i})}|}$ yields LDOS images consistent with calculated ones [9].

It should be emphasized that the Hamiltonian H is not a Hermitian operator for an eigenfunction $\psi_n(x)$ though $\partial^2/\partial x^2$ is a real operator and H does not have an imaginary part. This non-hermiticity comes from electron waves outgoing from the QC in regions I and V because we treat the case that an electron is supplied in region III. By using Dirac's notation, we obtain a non-zero surface integral; $\langle H\Psi_n|\Psi_n\rangle - \langle\Psi_n|H\Psi_n\rangle \neq 0$. Especially in the limit $t \to \infty$, we obtain

$$\begin{aligned}&\lim_{t\to\infty}[\langle H\Psi_n|\Psi_n\rangle - \langle\Psi_n|H\Psi_n\rangle]\\ &= -\frac{\hbar^2}{2m^*}\lim_{t\to\infty}\left[\Psi_n(x,t)\frac{\partial}{\partial x}\Psi_n^*(x,t)\right.\\ &\quad\left.-\Psi_n^*(x,t)\frac{\partial}{\partial x}\Psi_n(x,t)\right]\Bigg|_{x=-v_n^{(\mathrm{r})}t}^{x=v_n^{(\mathrm{r})}t} = \mathrm{i}\Gamma_n, \end{aligned}\tag{8}$$

where $v_n^{(\mathrm{r})} = \hbar k_n^{(\mathrm{r})}/m^*$. Eigenenergies, therefore, become complex numbers. When $\Gamma_n = 0$ which corresponds to the case of a stationary state, the Hamiltonian is Hermitian.

2.2. Two-dimensional quasi-stationary state

Here we consider an electron confined in a rectangular QC. We use a potential energy defined as

$$\begin{aligned}V(\boldsymbol{\rho}) = &-V_0 + (V_0 - V_1)[\theta(|x| - \tfrac{1}{2}a_x)\theta(\tfrac{1}{2}b_x - |x|)\\ &+ \theta(|y| - \tfrac{1}{2}a_y)\,\theta(\tfrac{1}{2}b_y - |y|)],\end{aligned}\tag{9}$$

where $\boldsymbol{\rho}$ is a position vector (x, y), the origin $(0, 0)$ is set at the center of the well and $\theta(x)$ represents Heaviside's function; $\theta(x) = 1$ for $x > 0$ and $\theta(x) = 0$ for $x < 0$. Figure 3 shows a schematic 3D image of this potential energy. The well has the inner width a_x in the x direction and a_y in the y direction. The rectangular potential energy has four barriers with the width $(b_x - a_x)/2$ in the x direction and the width $(b_y - a_y)/2$ in the y direction. To apply our model to the experimental system built up by Kliewer *et al* [9], a rectangular QC constructed with Mn atoms on an Ag(111) surface, we chose the bottom of the potential to be $-V_0 = -4.802$ eV and the level of four long bars to be $-V_1 = -4.350$ eV. We set the effective mass of the confined electron equal to $m^* = 0.42\,m_\mathrm{e}$ [9]. Four pillars shown in figure 3 have negligible effect on confined electrons because wavefunctions have low intensities near four corners.

Table 1. Values of ε_{nm} (meV).

	m				
n	1	2	3	4	5
1	−46.6	−25.1	12.2	66.3	137.8
2	−20.5	1.0	38.3	92.4	163.9
3	25.1	46.6	83.9	138.0	209.5
4	91.6	113.1	150.4	204.5	276.0
5	179.5	201.0	238.0	292.4	363.9

Because a Shockley-electron band of the Ag(111) surface intersects with the bulk band at about 400 meV [1], the Shockley electron having the lower energy stays mainly in a two-dimensional QC. We consider a situation where a rectangular QC confines such a Shockley electron. By using a separation-of-variables method, we assign the wavefunction confined in the QC as $\Psi_{nm}(\boldsymbol{\rho}) = \psi_n(x)\,\psi_m(y)$ in which $\psi_n(x) = D_n\sin k_n x + F_n\cos k_n x$ and $\psi_m(y) = D_m\sin k_m y + F_m\cos k_m y$. Eigenvalues k_n and k_m are solutions of two kinds of equations (3) and (4), and they are complex numbers written as $k_n = k_n^{(\mathrm{r})} + \mathrm{i}k_n^{(\mathrm{i})}$ and $k_m = k_m^{(\mathrm{r})} + \mathrm{i}k_m^{(\mathrm{i})}$. The eigenenergy can be written as $E_{nm} = E_{nm}^{(\mathrm{r})} - \mathrm{i}\frac{1}{2}\Gamma_{nm}^{\mathrm{QC}}$, where

$$E_{nm}^{(\mathrm{r})} = \frac{\hbar^2}{2m^*}[k_{nx}^{(\mathrm{r})^2} + k_{my}^{(\mathrm{r})^2} - k_{nx}^{(\mathrm{i})^2} - k_{my}^{(\mathrm{i})^2}] - V_0, \tag{10}$$

and

$$\Gamma_{nm}^{\mathrm{QC}} = -\frac{2\hbar^2}{m^*}[k_{nx}^{(\mathrm{r})}k_{nx}^{(\mathrm{i})} + k_{my}^{(\mathrm{r})}k_{my}^{(\mathrm{i})}]. \tag{11}$$

The $\hbar/\Gamma_{nm}^{\mathrm{QC}}$ is the lifetime of an electron associated with tunneling through four barriers because the probability density decays exponentially with time as $\exp(-\Gamma_{nm}^{\mathrm{QC}}t/\hbar)$ in the QC. Hereafter we label a state the (n, m) state. Odd numbers n and m refer to symmetric wavefunctions and even numbers refer to antisymmetric wavefunctions. Table 1 shows eigenenergies $\varepsilon_{nm} = E_{nm}^{(\mathrm{r})} - E_\mathrm{F}$ obtained for a rectangular QC fabricated by Kliewer *et al* [9] where the Fermi level is set at $E_\mathrm{F} = -4.740$ eV [18]. We solved eigenvalue equations by using $a_x = 90$ Å $- d$, $b_x = 90$ Å $+ d$, $a_y = 100$ Å $- d$ and $b_y = 100$ Å $+ d$ in which $d = 2.74$ Å. Since $a_x < a_y$ and $b_x < b_y$, we have a relation $\varepsilon_{nm} > \varepsilon_{mn}$ in the case that $n > m$. The ε_{nm} does not monotonically increase with n or m.

3. Scanning tunneling spectrum

3.1. LDOS and STS

The differential conductance of the STM current provides the surface local density of states (LDOS). The STS is proportional to the LDOS measured at a fixed position where the distance between the tip and the specimen is kept constant [5, 9]. In the present treatment, the effect of the DOS of the STM tip is thought to be negligible because the bias voltage is low and the bandwidth of a Shockley electron is small, which is in contrast to the case where we observe STM images of semiconductor

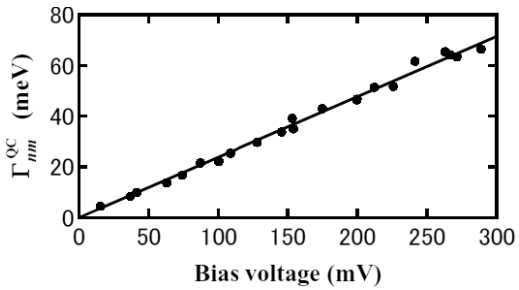

Figure 4. Energy width Γ_{nm}^{QC} as a function of $(E_{nm}^{(r)} + V_0)/e$. A fitting curve is shown as a straight line.

surfaces with bias voltages greater than 1 eV. Here we define the LDOS for electrons confined in a rectangular QC as [14]

$$D(\boldsymbol{\rho}, E) = \sum_{\sigma nm} |\Psi_{nm}(\boldsymbol{\rho})|^2 \frac{\Gamma_{nm}}{2\pi[(E - E_{nm}^{(r)})^2 + (\frac{1}{2}\Gamma_{nm})^2]}$$
$$= \sum_{\sigma nm} D_{nm}(\boldsymbol{\rho}, E), \qquad (12)$$

where σ represents spin degrees of freedom. The $D_{nm}(\boldsymbol{\rho}, E_F + eV)$ has a Lorentzian shape whose full width at half-maximum of the (n, m) state is Γ_{nm}. Considering that a Shockley electron originally has a lifetime on the clean surface, we set the energy width of a state (n, m) equal to $\Gamma_{nm} = \Gamma_{nm}^{QC} + \Gamma_{CS}$, where Γ_{CS} is associated with a Shockley electron on the clean surface. Figure 4 represents Γ_{nm}^{QC} as a function of $(E_{nm}^{(r)} + V_0)/e$. Closed circles represent Γ_{nm}^{QC}. Scattering of data comes from the difference in lengths of two sides of a rectangle. By the least-squares method, a sequence of Γ_{nm}^{QC} can be approximated as $[0.24\,(E_{nm} + V_0) + 0.36]$ meV which is shown as a straight line in figure 4. This linearity is not universal. With the increase in barrier thickness, Γ_{nm}^{QC} shows a concave curve against bias voltage. The slope 0.24 is close to the value 0.2 used by Li *et al* [8] for a hexagonal Ag island on the Ag(111) surface.

We neglect other contributions attributable to Coulomb interactions between electrons and the energy resolution of an STS apparatus. In addition, we neglect electron–phonon interactions because Kliewer *et al* [9] measured the STS at 4.6 K.

Figure 5 shows our STS obtained at the center of a QC in which we adopted the value $\Gamma_{CS} = 3$ meV to reproduce the highest peak at -47 mV of the (1, 1) state. Peak positions and peak widths are consistent with the experimental ones [9]. The value of Γ_{11}^{QC} is too small to explain the experimental peak width, which supports our introduction of Γ_{CS}. All quantum numbers inserted in figure 5 are odd, reflecting that symmetric wavefunctions have finite intensities at the center. In figure 5 we also show LDOS components $D_{nm}(\mathbf{0}, E_F + eV)$ calculated at the center. The peak height of each state decreases with the increase in bias voltage because a peak height at $E = E_{nm}^{(r)}$ of the Lorentzian part is $2/(\pi\Gamma_{nm})$ and Γ_{nm} increases with $E_{nm}^{(r)}$. Moreover, the probability density $|\Psi_{nm}(\boldsymbol{\rho})|^2$ at a fixed position $\boldsymbol{\rho}$ gives an additional weight on each peak. The STS obtained at the center is composed mainly of (1, 1), (1, 3) and (3, 1) states since these states have high probability density at the center. In addition, (3, 3) and (1, 5) states form peaks at higher bias voltages. Differences in peak heights of (1, 3) and

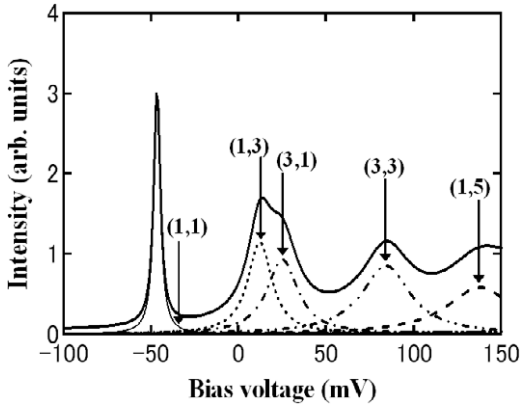

Figure 5. STS calculated at the center of a rectangle as a function of bias voltage. A thick curve shows $D(\mathbf{0}, E_F + eV)$ and other curves show components $D_{nm}(\mathbf{0}, E_F + eV)$.

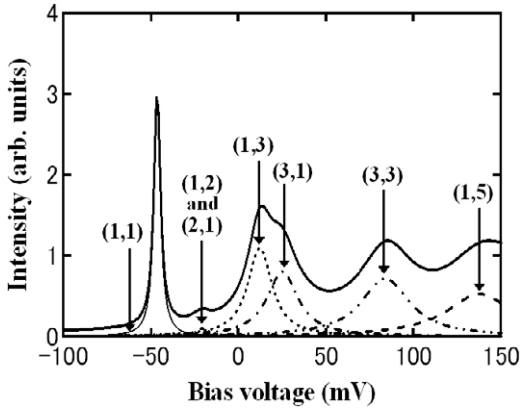

Figure 6. STS calculated at a position (4 Å, 2 Å) as a function of bias voltage.

(3, 1) states comes from the difference in side lengths of the rectangle resulting in relations $E_{13} < E_{31}$ and $\Gamma_{13}^{QC} < \Gamma_{31}^{QC}$. In this manner we can easily specify components of STS because each wavefunction has a rectangular symmetry. In contrast, Kliewer *et al* [9] obtained an overall profile of STS by using a scattering theory. In their analysis, the overall wavefunction is constructed by electron waves scattered circularly around each corral atom. Hence, it is difficult to pick out components of STS because scattered electrons have a circular symmetry.

Figure 6 shows our STS calculated at an off-centered position (4 Å, 2 Å). Because the (2, 1) state is antisymmetric with respect to the y axis and the (1, 2) state is antisymmetric with respect to the x axis, two peaks at -20.5 and -25.1 mV appear. Our STS is consistent with the experimental profile in both peak positions and the whole shape. Similarly to the STS calculated at the center, broad peaks at about $+20$ and $+85$ mV appear. Though Kliewer *et al* [9] gave a comment only on two peaks—the (1, 1) state for the highest peak at about -50 mV, and the (1, 2) state and (2, 1) state for the second peak at about -25 mV—our method gives more detailed information of peaks in all ranges of bias voltage.

In figures 5 and 6 dips between adjacent peaks show a gradual rise in height with bias voltage. This tendency is due

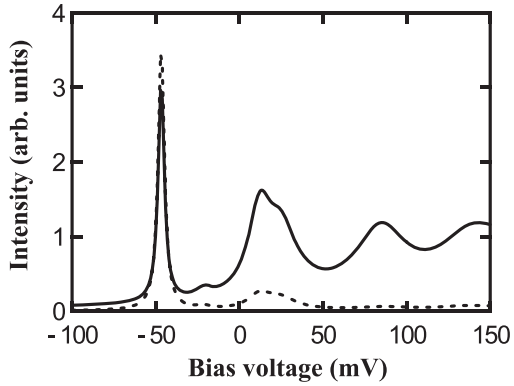

Figure 7. STS calculated by different normalization methods. A broken curve shows STS calculated in terms of δ-function normalization of wavefunctions. A solid curve shows STS shown in figure 6.

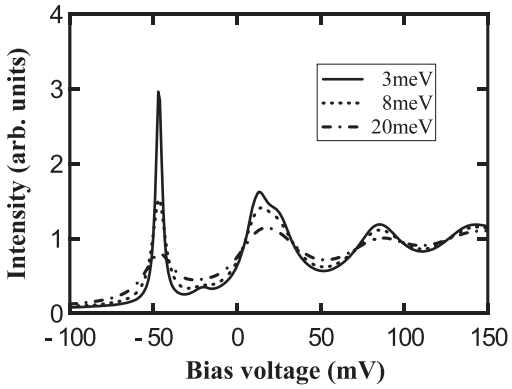

Figure 8. Γ_{CS} dependence of STS calculated at a position (4 Å, 2 Å).

to the relation $|A|^2 = |k^{(i)}|$ which yields an increase of $|D|$ and $|F|$ with eigenenergy. Finite intensities at dips, therefore, do not come from the background attributable to external factors such as energy resolution of an STM apparatus. We can determine coefficients D and F by another normalization method for wavefunctions so that the integration of probability densities over two regions outside the QC yields $\delta(k_{nx} - k'_{nx})\delta(k_{my} - k'_{my})$. In such a case, the values $|A|$ and $|J|$ become a constant which is independent of wavenumber k. A broken curve in figure 7 shows STS obtained by this normalization method. The profile is mostly structureless especially in the high energy range and is inconsistent with the experimental one though peak widths are consistent with experimental ones. A solid curve shows STS obtained by the normalization method considering the time evolution of wavefunctions; $|J_n|^2 = |A_n|^2 = |k_n^{(i)}|$ described in section 2.1. Because $|k_n^{(i)}|$ increases with $|E_n^{(r)}|$ and so does $|k_m^{(i)}|$ with $|E_m^{(r)}|$ and $|\Psi_{nm}(\boldsymbol{\rho})|^2$ is proportional to $|k_n^{(i)}| \times |k_m^{(i)}|$, the STS drawn by a solid curve is much higher than that drawn by a broken curve in the high bias-voltage range.

The effect of Γ_{CS} on electron states has been discussed on clean noble metal surfaces [19, 20]. Figure 8 shows Γ_{CS} dependence of the present STS calculated at the position $\boldsymbol{\rho} = (4\ \text{Å}, 2\ \text{Å})$. It clearly shows that the peak height of the highest peak decreases with the increase in Γ_{CS} and peaks at higher energy levels become dull. All peaks calculated with $\Gamma_{CS} = 20$ meV are broad and a peak at about -25 mV is absorbed into a wide dip. Hence, the value of Γ_{CS} should be less than 8 meV.

3.2. LDOS images

To clarify the relation between the STS and the LDOS image, we obtained the bias-voltage dependence of LDOS images. Figure 9 shows our LDOS images defined by $D(\boldsymbol{\rho}, E_F + eV)$ at bias voltages $V = \varepsilon_{nm}/e$. Two numerals in a bracket inserted in each subtitle represent the electron state (n, m). These images become complex with the increase in bias voltage. As is shown in equation (12), the image does not depend only on the state (n, m) but on electron states superposed over the energy range between E_F and $E_F + eV$.

3.3. Position dependence of STS

Figure 10 shows a position dependence of STS where scanning is carried out in the x direction from the center. A peak at -20 mV comes from the (2, 1) state, but the (1, 2) state does not form a peak because the LDOS image in figure 9(b) has low intensity near the x axis. A peak height at about $+12$ mV of the (1, 3) state decreases with the increase in distance from the center, and a peak height at about $+38$ mV of the (2, 3) state exceeds the peak height at about $+12$ mV. This tendency can be attributed to the difference between images in figures 9(e) and (g); a high intensity region exists near the center of figure 9(e) while a low intensity region exists near the center of figure 9(g). In the upper region of figure 10 a peak composed of (4, 1) and (2, 4) states appear at 90 mV. This can be explained by images of figures 9(j) and (k) in which high intensity regions are located near the right-hand side of a rectangle. A peak composed of (1, 3) and (3, 1) states disappears with the increase in scanning distance but a peak composed of (3, 3) and (4, 1) states appears instead. Peaks constructed with (2, 3) and (3, 2) states which are absent in figures 5 and 6 appear. With the further increase in scanning distance, a peak of the (3, 1) state reappears because of a bright area near the middle of the right-hand side of figure 9(f).

When the scanning is carried out along a diagonal line $y = (10/9)x$ (figure 11), a peak at 1 mV grows with the distance from the center. The cause is a bright spot near the upper right corner of figure 9(d). In addition to this, a peak at about -20 mV has a broader width than those in figure 10, which comes from a combination of two peaks at -25 and -20 mV. As the scanning position goes far from the center, peaks in figures 10 and 11 turn out to be dull because of large energy widths at high energy levels.

We should note that LDOS images can be obtained from the overall position dependence of STSs on condition that $z(\boldsymbol{\rho})$ is set to be a constant in which $\mathrm{d}I/\mathrm{d}V$ corresponds to LDOS.

3.4. Extraction of peak data from experimental STS

Besides an overall profile of STS, it is desirable to extract peak data from the experimental STS. Each peak width can be estimated by the second derivative with respect to V of

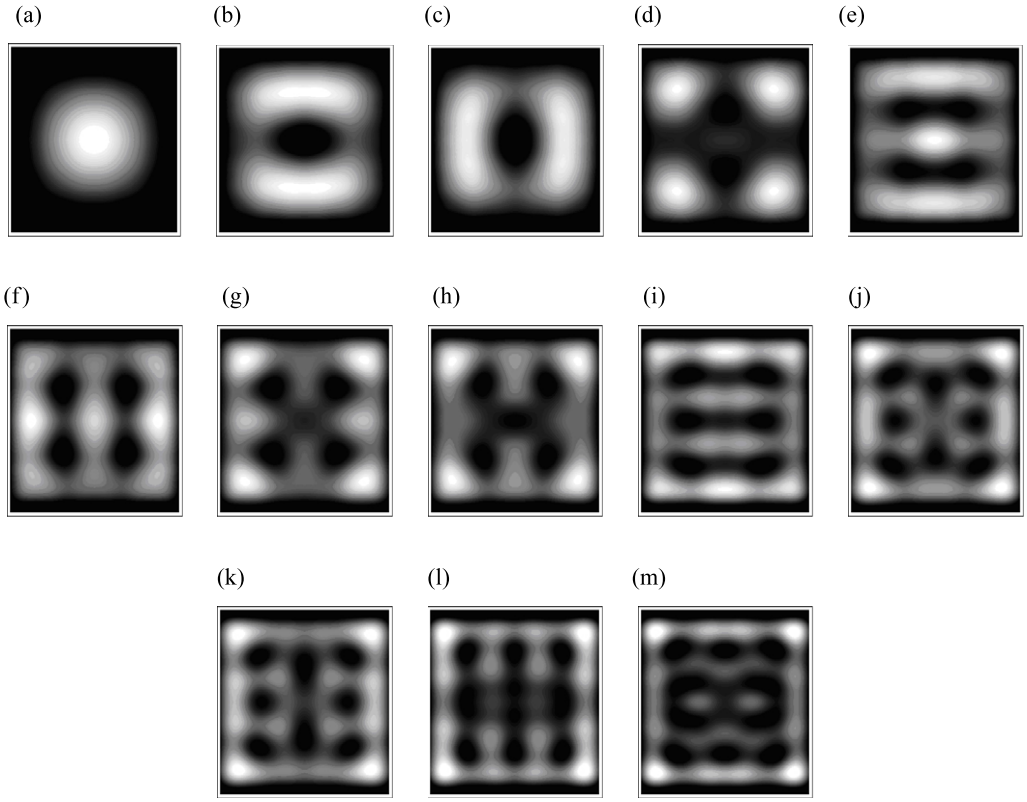

Figure 9. LDOS images calculated at eigenenergies $V = \varepsilon_{nm}/e$ (mV). The image at +92.6 mV is omitted because no apparent difference from that at +91.6 mV appears. (a) −46.6 mV (1, 1), (b) −25.1 mV (1, 2), (c) −20.5 mV (2, 1), (d) +1.0 mV (2, 2), (e) +12.2 mV (1, 3), (f) +25.1 mV (3, 1), (g) +38.3 mV (2, 3), (h) +46.6 mV (3, 2), (i) +66.3 mV (1, 4), (j) +83.9 mV (3, 3), (k) +91.6 mV (4, 1), (l) +113.1 mV (4, 2) and (m) +138.0 mV (3, 4).

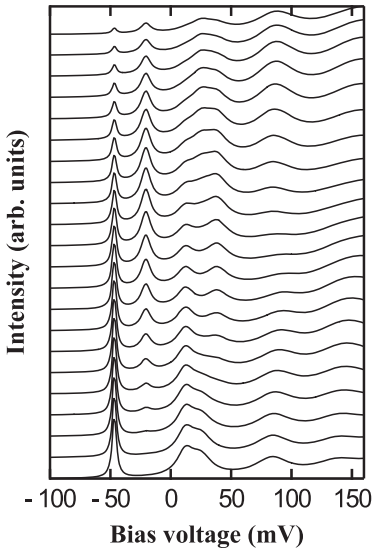

Figure 10. Position dependence of STS in the x direction. The increment in position is 2 Å. The uppermost curve shows STS calculated at a position (42 Å, 0 Å).

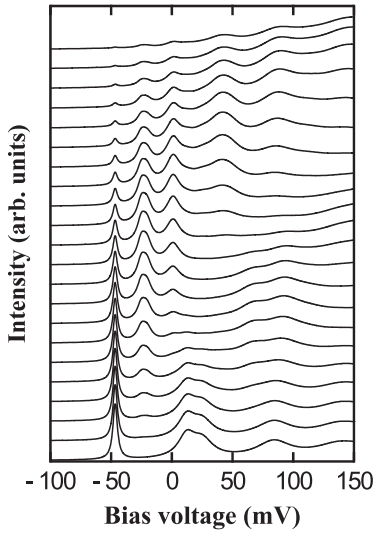

Figure 11. Position dependence of STS in a diagonal direction $y = (10/9)x$. The increment in position distance is 2 Å. The uppermost curve represents STS calculated at a position (42 Å, 46.7 Å).

STS. Figure 12 shows the second derivative of our STS shown in figure 6 as a function of bias voltage. We find zero points of $-\mathrm{d}^2 D_{nm}(\boldsymbol{\rho}, E_\mathrm{F} + eV)/\mathrm{d}V^2$ at a fixed position $\boldsymbol{\rho}$ as $eV_\pm = E^{(\mathrm{r})}_{nm} - E_\mathrm{F} \pm (\sqrt{3}/6)\Gamma_{nm}$ and the peak width can be estimated by the difference in adjacent zero points as $\Gamma_{nm} = \sqrt{3}e(V_+ - V_-)$. The peak profile is much sharper than that in figure 6 and each peak corresponds to that in STS. Although peaks in the STS are not fully separated, peaks in

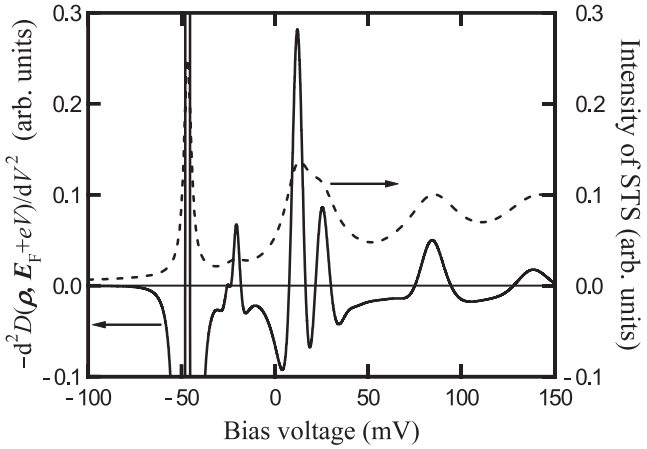

Figure 12. The second derivative of our STS profile with respect to bias voltage. A dashed curve represents the intensity of STS.

figure 11 are well separated. In figure 12, we find that a broad peak at about 25 mV displayed in figure 6 is split into two peaks and broad peaks at 90 and 140 mV become sharp peaks. Usually, an experimental intensity distribution is decomposed into Lorentzian components by choosing weighting constants and peak widths of them by a least-squares method, for example. Such a method, however, requires us to determine the number of peak components. We propose that the second derivative of the STS yields directly detailed information of STS components, which does not require uncertainty in choosing the number of peak components. To carry out the second derivative of the experimental STS it may actually require smoothing over the first derivative. Electron states of seven peaks in figure 12 can be assigned from the left as follows; (1, 1), (1, 2), (2, 1), (1, 3), (3, 1), (3, 3) and $(1, 5) + (3, 4)$. Energy widths taken from figure 12 are consistent with those obtained by $\Gamma^{QC}_{nm} + \Gamma_{CS}$ in which $\Gamma_{CS} = 3$ meV. We find that the first derivative is insufficient to acquire detailed information of peaks in STS because components are not well separated.

4. Discussion and conclusions

On the basis of scattering theory, as had been carried out by Kliewer *et al* [9], the LDOS is constructed by superposing circularly scattered waves. It is, therefore, difficult to specify electron states that have a rectangular symmetry. In that case it needs to refer to stationary states obtained for a box potential, for example. In addition to this, it needs to introduce energy widths as fitting parameters. Contrary to this, our viewpoint that electrons are in quasi-stationary states having a rectangular symmetry provides detailed information of eigenenergies and energy widths of a confined electron.

In conclusion, our results demonstrate that the STS for the electron confined in a rectangular QC can be explained by considering the electron to be in a quasi-stationary state. Such a viewpoint naturally yields peak widths of STS. Moreover, our treatment on STM images and STS enables us to clarify components of electron states contributing to STM images and STS. Hence, our results provide detailed information of confined electrons in both real space and energy space. As regards a method to determine eigenenergies and energy widths of the confined electron from an experimental STS, we propose that the second derivative of the STS with respect to a bias voltage provides detailed information of the confined electron.

References

[1] Kevan S D and Gaylord R H 1987 *Phys. Rev.* B **36** 5809
[2] Eigler D M and Scheweizer E K 1990 *Nature* **344** 524
[3] Stroscio J A and Eigler D M 1991 *Science* **254** 1319
[4] Crommie M F, Lutz C P and Eigler D M 1993 *Science* **262** 218
[5] Heller E J, Crommie M F, Lutz C P and Eigler D M 1994 *Nature* **369** 464
[6] Manoharan H C, Lutz C P and Eigler D M 2000 *Nature* **403** 512
[7] STM galleries from IBM Almaden Research Center Visualization Lab. Home page http://www.almaden.ibm.com/vis/stm/gallery.html
[8] Li J, Schneider W D, Berndt R and Crampin S 1998 *Phys. Rev. Lett.* **80** 3332
[9] Kliewer J, Berndt R and Crampin S 2001 *New J. Phys.* **3** 22.1
[10] Veuillen J V, Mallet P, Magaud L and Pons S 2003 *J. Phys.: Condens. Matter* **15** S2547
[11] Rieder K H, Meyer G, Braun K F, Hla S W, Moresco F, Morgenstern K, Repp J, Foelsch S and Bartels L 2003 *Europhys. News* **34** 95
[12] Diekhöner L, Schneider M A, Baranov A N, Stepanyuk V S, Bruno P and Kern K 2003 *Phys. Rev. Lett.* **90** 236801
[13] Fiete G A and Heller E J 2003 *Rev. Mod. Phys.* **75** 933 and references therein
[14] Kumagai T and Tamura A 2008 *J. Phys. Soc. Japan* **77** 014601
[15] Kumagai T and Tamura A 2008 *J. Phys.: Condens. Matter* **20** 285220
[16] Wells A F 1993 *Structural Inorganic Chemistry* 5th edn (Oxford: Oxford University Press) p 1288
[17] The Web Site of the American Chemical Society. Home page http://www.chemistry.org/portal/a/c/s/1/home.html and a further choice 'periodic table'
[18] Michaelson H B 1977 *J. Appl. Phys.* **48** 4729
[19] Kliewer J, Berndt R, Chulkov E V, Silkin V M, Echenique P M and Crampin S 2000 *Science* **288** 1399
[20] Eiguren A, Hellsing B, Reinert F, Nicolay G, Chulkov E V, Silkin V M, Hüfner S and Echenique P 2002 *Phys. Rev. Lett.* **88** 066805